

Article

Polar Order Evolutions near the Rhombohedral to Pseudocubic and Tetragonal to Pseudocubic Phase Boundaries of the BiFeO₃-BaTiO₃ System

Yongxing Wei ^{1,*}, Changqing Jin ¹, Yiming Zeng ², Xiaotao Wang ³, Gang Xu ¹ and Xiaoli Wang ³

Received: 31 July 2015; Accepted: 27 October 2015; Published: 2 December 2015

Academic Editor: Lorena Pardo

¹ School of Materials and Chemical Engineering, Xi'an Technological University, Xi'an 710021, China; eaglejin@xatu.edu.cn (C.J.); xugang@xatu.edu.cn (G.X.)

² State Key Laboratory of Advanced Technologies for Comprehensive Utilization of Platinum Metals, Kunming Institute of Precious Metals, Kunming 650106, China; zym@ipm.com.cn

³ MOE Key Laboratory for Non-equilibrium Synthesis and Modulation of Condensed Matter, School of Science, Xi'an Jiaotong University, Xi'an 710049, China; In.01211@stu.xjtu.edu.cn (X.W.); xlwang1@mail.xjtu.edu.cn (X.W.)

* Correspondence: weiyongxing@xatu.edu.cn; Tel.: +86-150-2924-7969

Abstract: Solid solutions of $(1-x)\text{BiFeO}_3-x\text{BaTiO}_3$ (BF-BT, $0.05 \leq x \leq 0.98$) were prepared and characterized. It was found that the dielectric constant ϵ_m , remnant polarization P_r and piezoelectric coefficient d_{33} reach their maximum values near the rhombohedral–pseudocubic phase boundary. In particular, the 0.7BF-0.3BT composition shows large polarization ($P_r > 20 \mu\text{C}/\text{cm}^2$) and a temperature-stable piezoelectric property ($d_{33} > 100 \text{ pC/N}$ when the annealing temperature is lower than $\sim 400^\circ\text{C}$). Near the tetragonal–pseudocubic phase boundary, ϵ_m and P_r decrease, and the piezoelectric property vanishes when the BF content reaches 4 mol %.

Keywords: morphotropic phase boundary; piezoelectric; BiFeO₃

1. Introduction

Bi-based perovskite materials, BiMeO₃ (BM), in which Me can be a single trivalent cation or a mixture of two cations, have been studied because of their high polarization and T_c values. However, synthesis of a single-phase BM perovskite ceramic material by conventional synthesized methods is challenging; this may be due to the small radius of the Bi cation [1–4]. The addition of PbTiO₃ (PT) or BaTiO₃ (BT) with large A-site ions into BM ceramics to form solid solutions can effectively stabilize the perovskite structure. Some BM-PT systems exhibit a large d_{33} piezoelectric coefficient with a high T_c near the morphotropic phase boundary (MPB) [5–8]. In particular, the piezoelectric activity in 0.36BiScO₃-0.64PbTiO₃ ($d_{33} > 460 \text{ PC/N}$, $T_c = 450^\circ\text{C}$) is comparable to that in the Pb(Zr_{1-x}Ti_x)O₃ (PZT) material [5]. On the other hand, for BM-BT systems, even the end members are both ferroelectrics with low symmetry structures (Bi(Ti_{1/2}Zn_{1/2})O₃-BaTiO₃, BiAlO₃-BaTiO₃, etc.), and the decrease in BT content leads to the appearance of the undesired pseudo-cubic phase. The composition-driven ferroelectric-relaxor transition is usually found near the phase boundary between the tetragonal (T) and pseudocubic (PC) phases [9–11]. On the BM side of the phase diagram, limited solubility gives rise to difficulty in studying the structures and electrical properties of these materials.

BiFeO₃-BaTiO₃ (BF-BT) was first investigated for its multiferroic properties [12–14]. A small amount of BT can effectively stabilize the perovskite phase [14]. Earlier investigations of the BF-BT system have shown that the system undergoes structural transitions, from the rhombohedral (R)

to the cubic (C) and to the T phase, with the addition of BT [12]. The observation of ferroelectric behavior in compositions with a BT content of 33 to 50 mol % suggests that the intermediate phases might be considered to have PC symmetry [15–17]. Recently, good piezoelectric properties near the rhombohedral–pseudocubic (R-PC) phase boundary have been found in unmodified 0.7BF-0.3BT ceramics ($d_{33} = 134$ pC/N) and Mn-modified 0.725BF-0.275BT ceramics ($d_{33} = 136$ pC/N) [18–20]. Near the tetragonal–pseudocubic (T-PC) phase boundary, a smeared dielectric anomaly has been found in 0.04BF-0.96BT ceramics, with a maximum dielectric constant ϵ_m of ~800, but the related ferroelectric and piezoelectric properties have rarely been reported [21,22].

To understand the polar order mechanism of BF-BT, systematic investigations of electrical properties in the BF-BT system should be carried out. In this work, $(1-x)$ BF- x BT ($0.05 \leq x \leq 0.98$) solid solution ceramics were prepared. The different polarization behaviors near the R-PC and T-PC phase boundaries were reported and discussed.

2. Experimental Methods

The $(1-x)$ BF- x BT ($0.05 \leq x \leq 0.98$) solid solution ceramics were prepared using the mixed oxide method. The starting reagents of Bi_2O_3 (>99%) (Sinapharm Chemical Reagent Co., Ltd, Shanghai, China), Fe_2O_3 (>99%) (Sinapharm Chemical Reagent Co., Ltd.), BaCO_3 (>99%) (Sinapharm Chemical Reagent Co., Ltd.) and TiO_2 (>99%) (Sinapharm Chemical Reagent Co., Ltd.) were carefully weighed in stoichiometric ratios and wet mixed thoroughly by ball-milling for 10 h. The mixture was then dried and calcined at 750–1140 °C (Table 1) for 2 h in a cove red corundum crucible. The calcined powder was ball-milled and dried. Pellets with a diameter and thickness of 12 and 1–2 mm, respectively, were pressed using a 10% polyvinyl alcohol binder. The pellets were sintered in a covered corundum crucible at 930–1340 °C (Table 1) for 3 h. To reduce the volatilization of bismuth oxide during sintering, the pellets were buried with the mixture of Bi_2O_3 and calcined ZrO_2 . For X-ray diffraction measurements, the ceramics were crushed into fine powders. For electric measurements, silver paste was painted onto both sides of the ground ceramic pellets and fired at 810 °C for 10 min. Prior to the piezoelectric measurements, the ceramics were poled under 35–70 kV/cm in silicone oil for 10 min at room temperature.

Table 1. Calcination and sintering temperatures of $(1-x)\text{BiFeO}_3$ - BaTiO_3 ((1- x)BF- x BT) system.

Compositions	Temperature (°C)	
	Calcination	Sintering
0.95BF-0.05BT	750	930
0.9BF-0.1BT	750	960
0.8BF-0.2BT	750	980
0.75BF-0.25BT	800	990
0.7BF-0.3BT	800	1000
0.65BF-0.35BT	800	1050
0.6BF-0.4BT	800	1050
0.55BF-0.45BT	850	1090
0.5BF-0.5BT	900	1100
0.4BF-0.6BT	950	1140
0.2BF-0.8BT	1000	1220
0.1BF-0.9BT	1080	1260
0.04BF-0.96BT	1140	1340
0.02BF-0.98BT	1140	1340

Crystal structures of $(1-x)$ BF- x BT ceramics were detected using an X-ray diffractometer (XRD, Bruker AXS D8 ADVAMDMCE, Karlsruhe, German). The lattice parameters were refined based on XRD patterns using the Rietveld method, as implemented in the Topas 4.2 software. The space groups for compositions with $0.1 \leq x \leq 0.3$, $0.3 < x \leq 0.9$ and $0.9 < x \leq 0.98$ were chosen as rhombohedral

R3c, cubic Pm $\bar{3}m$, and tetragonal P4mm, respectively. The dielectric measurements were performed using an automated system, with a temperature-controlled sample chamber and an Agilent 4284A LCR meter controlled by a personal computer. The ferroelectric hysteresis loop was measured using an automatic ferroelectric test system [23]. The applied electric field signal is sinusoidal with the frequency of 10 Hz. The d_{33} values were measured using a piezo- d_{33} meter (ZJ-3AN; Institute of Acoustics, Beijing, China).

Structural and dielectric measurements of unpoled and poled ceramics for 0.7BF-0.3BT, 0.65BF-0.35BT and 0.6BF-0.4BT were performed. The ceramics were poled for 10 min at room temperature. Structural and dielectric measurements of poled ceramics were carried out after 24 h. Both the unpoled and poled ceramics were polished for structural measurements.

3. Results and Discussion

The diffraction peaks of all of the compositions could be indexed as a single perovskite structure, with no observed impure phase (see the Supplementary Information).

3.1. Structural and Electrical Properties near the R-PC Phase Boundary

Figure 1 shows the XRD patterns, temperature dependences of the dielectric constant ϵ , and polarization hysteresis loops for 0.8BF-0.2BT, 0.7BF-0.3BT and 0.55BF-0.45BT ceramics. According to the splitting of $\{110\}_c$ and $\{111\}_c$ reflections (Figure 1a), the 0.8BF-0.2BT ceramic most likely exhibits a highly distorted rhombohedral structure, while the 0.7BF-0.3BT ceramic shows a weak rhombohedral distortion. No clear splitting of $\{110\}_c$ and $\{111\}_c$ reflections was found in the compositions with a BT content larger than 30 mol %.

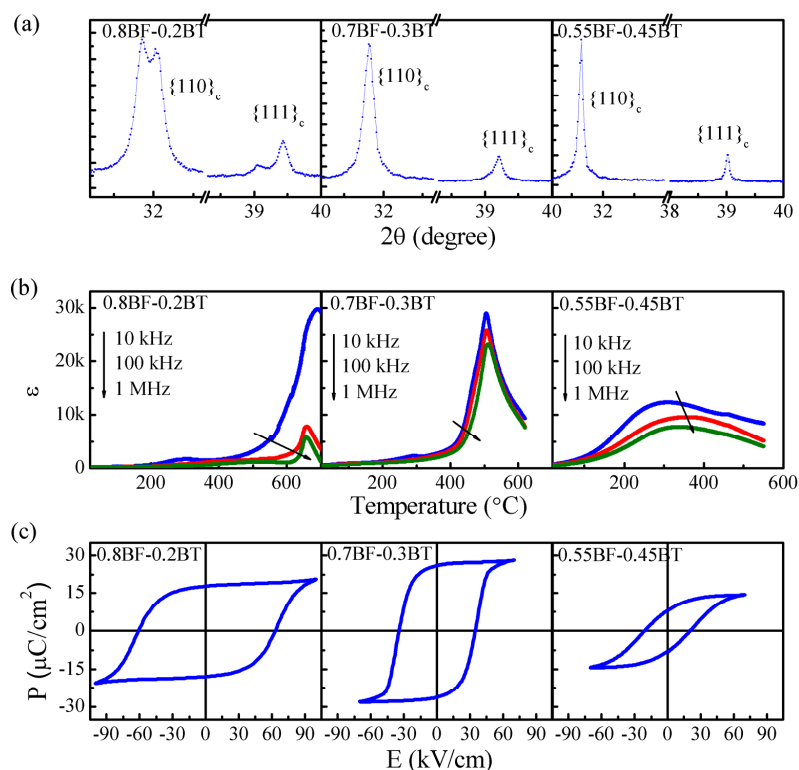


Figure 1. Structural and electrical properties of the BF-BT system near the BF side. (a) X-ray diffractometer (XRD) patterns; (b) temperature dependence of the dielectric constant ϵ (1 MHz); and (c) polarization hysteresis curves of 0.8BF-0.2BT, 0.7BF-0.3BT and 0.55BF-0.45BT ceramics.

Figure 1b shows that the 0.8BF-0.2BT ceramic exhibits a sharp dielectric peak at ~ 657 °C. The temperature T_m for the dielectric peak is frequency-independent. However, no endothermic or exothermic peak could be found near T_m (Figure 2). Furthermore, the temperature dependence of the structures also indicates the coexistence of the rhombohedral and cubic structures over a 100 °C range around T_m [35]. It may therefore be reasonable to suggest that 0.8BF-0.2BT is ferroelectric with the diffuse phase transition. The dielectric constant of 0.7BF-0.3BT increases abruptly for temperature higher than 400 °C. The dielectric anomaly is broad, with a maximum value $\epsilon_m > 20,000$. The corresponding T_m is frequency-dependent. This suggests that the high-temperature dielectric behavior of 0.7BF-0.3BT may be relaxor-like. The 0.55BF-0.45BT ceramic displays a frequency-dependent and very diffuse dielectric anomaly, with a ϵ_m of 7780 at 1MHz, and the dielectric constant above T_m decreases slowly with increasing temperature. Accordingly, the increasing level of BT substitution leads to a tendency to increase the structural disorder and increase the diffuseness of the dielectric anomaly.

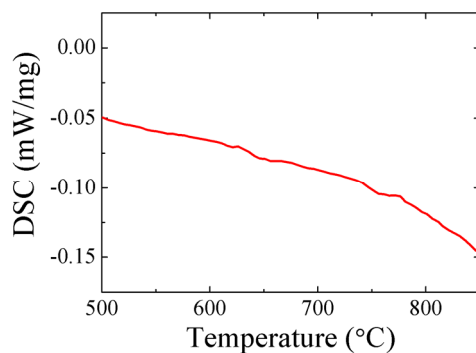


Figure 2. Differential scanning calorimetry (DSC) curve of 0.8BF-0.2BT.

The 0.8BF-0.2BT and 0.7BF-0.3BT ceramics show normal polarization switching behavior at room temperature (Figure 1c). Considering the dielectric and ferroelectric data, it is possible that 0.7BF-0.3BT displays a temperature-driven ferroelectric-relaxor transition. A slim ferroelectric hysteresis loop was found for the 0.55BF-0.45BT ceramic, possibly indicating the presence of the relaxor state.

The composition dependences of the dielectric, ferroelectric, and piezoelectric properties for the BF-BT system are shown in Figure 3. For compositions with rhombohedral distortions, the values of room-temperature ϵ and ϵ_m increase with increasing BT content (Figure 3a,b). The largest ϵ_m is found for the composition near the phase boundary. Due to the large E_c , 0.8BF-0.2BT and 0.75BF-0.25BT ceramics were not poled to saturation. This means that the measured P_r may be lower than the intrinsic values. The addition of BT induces decreases in E_c , confirming the transition from hard ferroelectrics to soft ferroelectrics (Figure 3c) [18,19]. The 0.7BF-0.3BT ceramic exhibits optimum ferroelectric and piezoelectric properties (Figure 3d,e). For compositions with a pseudo-cubic structure, the values of ϵ_m , P_r and d_{33} all decrease with the increasing BT content.

Table 2 lists the ferroelectric and piezoelectric parameters for the 0.7BF-0.3BT system, pure BF ceramic, and other BF-based systems [1,24–34]. The pure BF ceramic exhibits a very high T_c and d_{33} of 44 pC/N [1,25]. Introducing rare earth ions with the same valence at the BF A-site does not result in an enhancement of the piezoelectric property [25–29]. This may be caused by the large E_c . Solid solution systems of BF-BT, BF-PT and BiFeO₃-(Bi_{0.5}K_{0.5})TiO₃ contain two cations with different valences on both the A-site and B-site. However, the value of d_{33} for the BiFeO₃-PbTiO₃ and BiFeO₃-(Bi_{0.5}K_{0.5})TiO₃ systems is not higher than 100 pC/N [30,31]. Excellent piezoelectric performance is found for compositions of the modified BF-PT systems [32,34]. Interestingly, the compositions of the modified BF-PT systems and 0.7BF-0.3BT all have weak ferroelectric distortion, with a relatively low E_c .

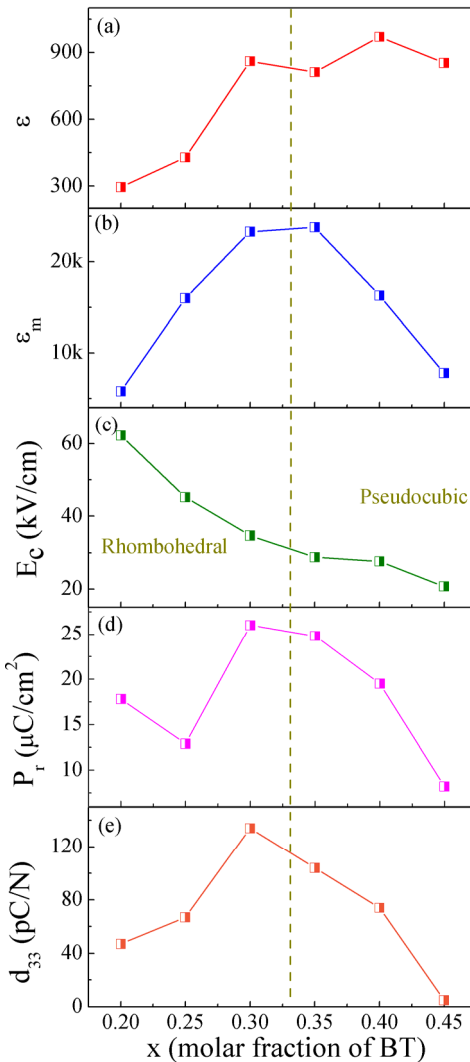


Figure 3. (a) Room-temperature ϵ ; (b) maximum dielectric constant ϵ_m ; (c) coercive field E_c ; (d) remnant polarization P_r ; and (e) piezoelectric coefficient d_{33} as a function of the BT content for the BF-BT system.

Table 2. Ferroelectric and piezoelectric properties of 0.7BF-0.3BT, BiFeO₃ (BF) and other BF-based ceramics.

Compositions	P_r ($\mu\text{C}/\text{cm}^2$)	E_c (kV/cm)	d_{33} (pC/N)	T_c/T_m (°C)	References
0.7BF-0.3BT	26.0	34.6	134	511	-
BF	~13	>50	44	830~850	[1,24]
Bi _{0.92} Dy _{0.08} FeO ₃	25.2	>100	37	-	[25]
Bi _{0.875} Sm _{0.125} FeO ₃	15.1	>80	29	-	[26]
Bi _{0.91} La _{0.05} Tb _{0.04} FeO ₃	-	-	9	-	[27]
Bi _{0.85} La _{0.15} FeO ₃	12.1	>60	28	-	[28]
(Bi _{1-x} Nd _x)FeO ₃ ($x = 0\text{--}0.15$)	-	-	26~28	-	[29]
0.675BiFeO ₃ -0.325PbTiO ₃	62	>40	85	642	[30]
0.6BiFeO ₃ -0.4(Bi _{0.5} K _{0.5})TiO ₃	~15	~40	37	441	[31]
0.57(Bi _{0.8} La _{0.2})(Ga _{0.05} Fe _{0.95})O ₃ -0.43PbTiO ₃	~30	~20	295	264	[32]
0.511BiFeO ₃ -0.326PbZrO ₃ -0.163PbTiO ₃	~12	~40	101	431	[33]
0.33BiFeO ₃ -0.2BaZrO ₃ -0.47PbTiO ₃	~30	~20	~270	270	[34]

The annealing temperature dependence of d_{33} for 0.7BF-0.3BT is shown in Figure 4. The d_{33} was measured after the sample was annealed at selected temperatures for one hour. The value of d_{33} is

stable with respect to temperatures below ~ 400 °C (>100 pC/N) and then drops noticeably around the depolarization temperature T_d . The T_d of 0.7BF-0.3BT is ~ 420 °C, which is much higher than that of the lead-free ($\text{Bi}_{0.5}\text{Na}_{0.5}$) TiO_3 -based ceramics [36].

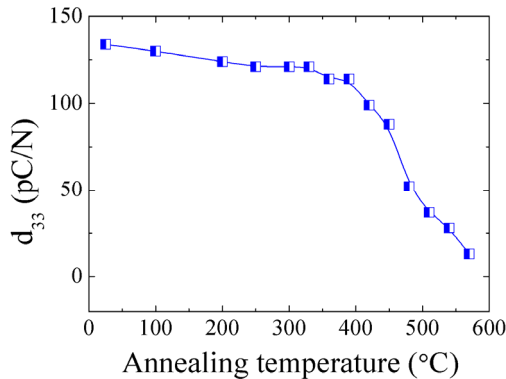


Figure 4. Annealing temperature dependence of room-temperature d_{33} for 0.7BF-0.3BT.

Figure 5 shows the XRD patterns and the temperature dependence of ϵ for unpoled and poled BF-BT ceramics near the R-PC phase boundary. Clear splits of $\{111\}_c$ reflection were found in 0.7BF-0.3BT after poling. This suggests that the electric field triggers an obvious modification of the lattice parameters in 0.7BF-0.3BT. However, the crystal symmetry does not change after poling. This shows that the electric-field-induced phenomenon in 0.7BF-0.3BT may be different from that in MPB-based system [37,38]. The possible polarization directions ($\langle 111 \rangle_c$ directions) could be only related to the rhombohedral distortion. Furthermore, the value of ϵ_m for the poled 0.7BF-0.3BT is much larger than that for the unpoled sample (Figure 5b). On the other hand, for 0.65BF-0.35BT and 0.6BF-0.4BT, there are no obvious differences in the structure and ϵ_m before and after poling. The detailed structure data are shown in the Supplemental Information.

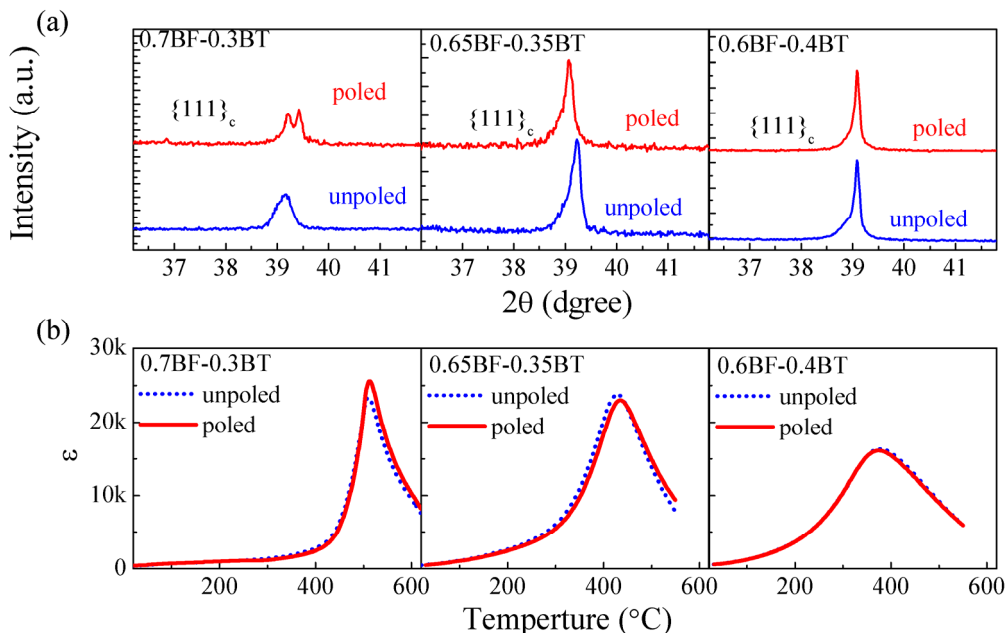


Figure 5. (a) XRD patterns; (b) Temperature dependence of the dielectric constant ϵ of unpoled and poled samples for BF-BT compositions across the rhombohedral-pseudocubic phase boundary.

3.2. Structural and Electrical Properties near the T-PC Phase Boundary

The XRD patterns, temperature dependences of dielectric properties, and polarization hysteresis loops of 0.02BF-0.98BT and 0.04BF-0.96BT ceramics are shown in Figure 6. Clear splitting of the $\{200\}_c$ peak reflections for the 0.02BF-0.98BT ceramic reveals the presence of a tetragonal distortion (Figure 6a). However, for the 0.04BF-0.96BT ceramic, the splitting of $\{200\}_c$ reflections is much weaker. This suggests that the tetragonal distortions are effectively suppressed when BF content reaches 4 mol %.

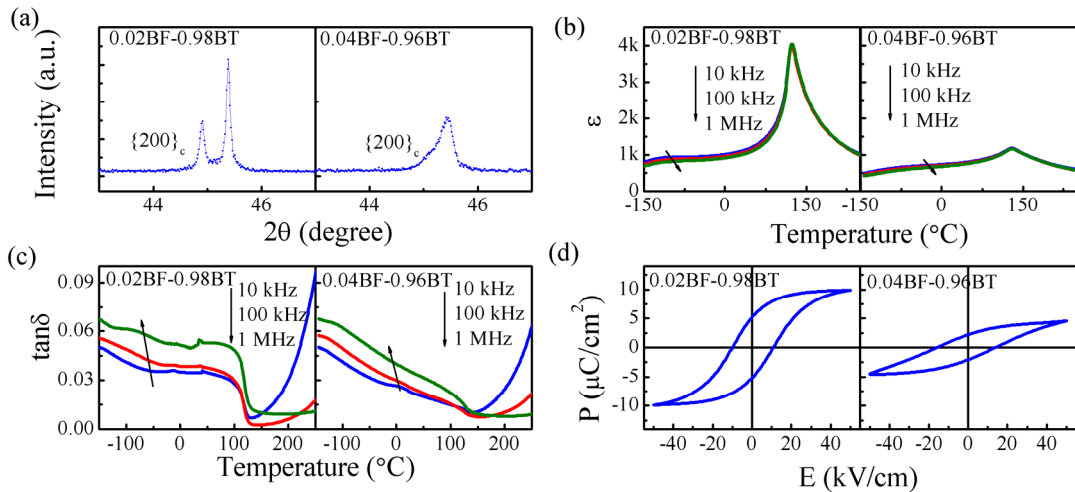


Figure 6. Structural and electrical properties of the BF-BT system near the BT side. (a) XRD patterns; (b) temperature dependence of dielectric constant ϵ ; (c) temperature dependence of dielectric loss $\tan\delta$; and (d) polarization hysteresis curves of 0.02BF-0.98BT and 0.04BF-0.96BT ceramics.

The 0.02BF-0.98BT ceramic exhibits a sharp dielectric peak near 123°C , with a ϵ_m of 4300 (Figure 6b). The corresponding T_m is frequency-independent. The sharp dielectric peak can be related to the transition from the ferroelectric T phase to the paraelectric C phase. Additionally, 0.02BF-0.98BT displays another weak and broad dielectric anomaly around -130°C . As is known, pure BT ceramic has two dielectric anomalies below room temperature that are related to the tetragonal-orthorhombic and orthorhombic-rhombohedral phase transitions. The low temperature dielectric behavior of 0.02BF-0.98BT suggests that a small amount of BF content weakens the low-temperature phase transitions of BT. The dielectric anomaly of 0.04BF-0.96BT is smeared ($\epsilon_m = 1170$), with a frequency-independent T_m . The $\tan\delta$ value for 0.02BF-0.98BT decreases abruptly near T_m (Figure 6c). On the other hand, the decrease in $\tan\delta$ near T_m for 0.04BF-0.96BT is gradual. The dielectric data of 0.04BF-0.96BT may suggest the diffused phase transition [21].

The ferroelectric behaviors of 0.02BF-0.98BT and 0.04BF-0.96BT ceramics are also different (Figure 6d). A normal ferroelectric hysteresis loop is observed in the former, with a P_r of $5.3 \mu\text{C}/\text{cm}^2$, while a slim hysteresis loop is found in the latter, with a P_r of $2.2 \mu\text{C}/\text{cm}^2$. The value of d_{33} for 0.02BF-0.98BT is 14 pC/N . However, d_{33} vanishes for 0.04BF-0.96BT. The evolutions of the dielectric, ferroelectric, and piezoelectric properties near the BT end member reveal that long-range ferroelectric order is destroyed when the BF content is 4 mol %.

3.3. Composition Dependence of Lattice Parameters

Figure 7 shows the lattice parameters of BF-BT ceramics as a function of the BT content. The ferroelectric distortion near the BT side is much more easily disrupted than that near the BF side. In the tetragonal region, the c_T value for 0.04BF-0.96BT (4.009 \AA) decreased significantly relative to that for 0.02BF-0.98BT (4.034 \AA), while the a_T values of the two compositions are similar. The reduction of the c axis leads to the suppression of the tetragonal distortion. The calculated lattice

parameters for the rhombohedral BF-BT compositions are described in the hexagonal unit cell with the R3c space group. To clearly observe the rhombohedral distortion, the lattice parameters in the perovskite-type unit cell are used. The transformation relation could be expressed as:

$$a_r = \frac{1}{3} \sqrt{3a_H^2 + \left(\frac{c_H}{2}\right)^2} \quad (1)$$

$$\sin \frac{\alpha}{2} = \frac{3}{2} \frac{1}{\sqrt{3 + \left(\frac{c_H}{2a_H}\right)^2}} \quad (2)$$

where a_H and c_H are the lattice parameters in the hexagonal unit cell and a_r and α are the lattice parameter and rhombohedral angle in the perovskite-type unit cell, respectively. The values of α and a_r both increase gradually with the addition of BT. When the BT content is 25 mol %, the composition still shows a large rhombohedral distortion ($\alpha = 89.68^\circ$).

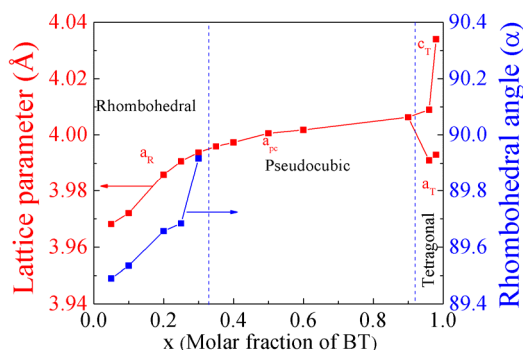


Figure 7. Lattice parameters of the BF-BT system as a function of the BT content.

3.4. Possible Reasons for the Different Behaviors near the Two Phase Boundaries

It is known that both temperature-driven polymorphic structure transitions (e.g., BT-based ceramics, $(K_xNa_{1-x})NbO_3$ based ceramics) and composition-driven MPB (e.g., $Pb(Zr_xTi_{1-x})O_3$, $Pb(Mg_{1/3}Nb_{2/3})O_3$ - $PbTiO_3$) can improve the piezoelectric activity [36,39–42]. Although most MPBs are related to the transitions between the R phase and T phase, the composition-driven R-C or T-C transition may also lead to the enhancement in electrical properties [39]. The phase boundary (separation of the R phase and PC phase) for the BF-BT system could be regarded as MPB. Near the MPB, the BF-BT system shows a temperature-driven and composition-driven ferroelectric-relaxor transition, which is similar to that in $Pb(Mg_{1/3}Nb_{2/3})O_3$ - $PbTiO_3$ [41]. However, no clear ferroelectric distortions could be found in the unpoled compositions that show the enhanced electrical properties.

Near the T-PC phase boundary, when the content of BF is only 4 mol %, the tetragonal distortions and long-range ferroelectric order are effectively suppressed. The electrical behaviors near the two phase boundaries in the BF-BT system are quite different. The mixtures of atoms with different electronegativities, valences, and radii both on the A-site and B-site, coupled with the structural inhomogeneity, increase the complexity of the structure-property relation. However, two important factors should be considered.

First, the Bi(6s)-O(2p) covalent bonds are much stronger than the Ti(4d)-O(2p) covalent bonds. The Ti cation displacement in BT along the $[001]_c$ direction from the central of ideal cubic perovskite is ~ 0.14 Å [43]. For BF, the Bi cation displacement along the $[111]_c$ direction is ~ 0.676 Å [44]. This may suggest that the Ti-O covalent bond is more easily weakened than the Bi-O covalent bond.

In addition, the effects of the structure parameters near the BF and BT sides are also different. Near the BF side, the addition of Ba^{2+} ions with a large radius expands the unit cell, as shown by the compositional dependence of the lattice parameters (Figure 7). The displacement space of the Bi^{3+}

ions is enlarged. Large off-center displacements could be present in Bi-rich regions. As a result, large polarization is possible near the R-PC phase boundary of the BF-BT system. A similar effect has been reported in the $\text{Ba}(\text{Ti}_{1-x}\text{Sn}_x)\text{O}_3$ system, in that the radii of the Sn^{4+} ions are much larger than those of the Ti^{4+} ions [45]. Although there are no reports on the electrical properties near the BM side in other BM-BT systems, a polarization enhancement is expected. Near the BT side, the addition of BF leads to the decrease in the length of c axis parameter. The displacement along the $[001]_c$ direction for the Ti^{4+} ions is reduced, as also shown by neutron diffraction data [21]. The similar phenomenon was observed in other BM-BT systems [9–11]. The reason for this is still unclear. Nevertheless, the types of A-site ions should be considered. For BM-PT systems that contain ferroelectric active Bi^{3+} and Pb^{2+} cations on the A-site, the behavior is different. The length of the c axis and the tetragonal distortion for $\text{BiScO}_3\text{-PbTiO}_3$ and $\text{Bi}(\text{Ti}_{1/2}\text{Mg}_{1/2})\text{O}_3\text{-PbTiO}_3$ systems near the PT side decrease slowly with the decreasing PT content [5,7]. In contrast, the addition of BF or $\text{Bi}(\text{Ti}_{0.5}\text{Zn}_{0.5})\text{O}_3$ leads to the increase in the c axis and the tetragonal distortion near the PT region [46,47]. A first-principles theoretical calculation should be carried out to further understand the two phase boundaries for BF-BT.

4. Conclusions

In conclusion, the polar order evolutions near the R-PC and T-PC phase boundaries in the BF-BT system are different. Near the R-PC phase boundary, 0.7BF-0.3BT exhibits a large polarization and a temperature-stable piezoelectric property ($T_d = \sim 420^\circ\text{C}$). The increase of BF content leads to the decrease of the electrical parameters near the BT side. The long-ranged ferroelectric order is disrupted when the BF content is only 4 mol %. An understanding of the electrical behaviors in the BF-BT system may help in the search for high-performance Pb-free piezoelectric ceramics based on similar phase boundaries.

Supplementary Materials: The following are available online at www.mdpi.com/1996-1944/8/12/5462/s1.

Acknowledgments: This work was financially supported by the National Natural Science Foundation of China (project No. 50772087 and 11404251) and the President's Fund of Xi'an Technological University (project No. XAGDXJJ111).

Author Contributions: Xiaoli Wang and Yongxing Wei designed the experiments. Yongxing Wei and Xiaotao Wang performed the experiments. Xiaoli Wang, Changqing Jin, Yiming Zeng and Gang Xu supplied the theoretical guidance. Yongxing Wei wrote the manuscript.

Conflicts of Interest: The authors declare no conflict of interest.

References

- Catalan, G.; Scott, J.F. Physics and applications of bismuth ferrite. *Adv. Mater.* **2009**, *21*, 2463–2485. [[CrossRef](#)]
- Belik, A.A.; Likubo, S.; Kodama, K.; Igawa, N.; Shamoto, S.; Maie, M.; Nagai, T.; Matsui, Y.; Stefanovich, S.Y.; Lazoryak, B.I.; et al. BiScO_3 : Centrosymmetric BiMnO_3 -type oxide. *J. Am. Chem. Soc.* **2006**, *128*, 706–707. [[CrossRef](#)] [[PubMed](#)]
- Suchomel, M.R.; Fogg, A.M.; Allix, M.; Niu, H.J.; Claridge, J.B.; Rosseinsky, M.J. $\text{Bi}_2\text{ZnTiO}_6$: A lead-free closed-shell polar perovskite with a calculated ionic polarization of $150\text{ }\mu\text{C}/\text{cm}^2$. *Chem. Mater.* **2006**, *18*, 4987–4989. [[CrossRef](#)]
- Khalyavin, D.D.; Salak, A.N.; Vyshatko, N.P.; Lopes, A.B.; Olekhnovich, N.M.; Pushkarev, A.V.; Maroz, I.I.; Radyush, Y.V. Crystal structure of metastable perovskite $\text{Bi}(\text{Mg}_{1/2}\text{Ti}_{1/2})\text{O}_3$: Bi-based structural analogue of antiferroelectric PbZrO_3 . *Chem. Mater.* **2006**, *18*, 5104–5110. [[CrossRef](#)]
- Eitel, R.E.; Randall, C.A.; Shrout, T.R.; Park, S.E. Preparation and characterization of high temperature perovskite ferroelectrics in the solid-solution $(1-x)\text{BiScO}_3-x\text{PbTiO}_3$. *Jpn. J. Appl. Phys.* **2002**, *41*, 2099–2104. [[CrossRef](#)]
- Alguero, M.; Ramos, P.; Jimenez, R.; Amorin, H.; Vila, E.; Castro, A. High temperature piezoelectric $\text{BiScO}_3\text{-PbTiO}_3$ synthesized by mechanochemical methods. *Acta Mater.* **2012**, *60*, 1174–1183. [[CrossRef](#)]

7. Randall, C.A.; Eitel, R.E.; Jones, B.; Shrout, T.R.; Woodward, D.I.; Reaney, I.M. Investigation of a high T_c piezoelectric system: $(1-x)\text{Bi}(\text{Mg}_{1/2}\text{Ti}_{1/2})\text{O}_3-x\text{PbTiO}_3$. *J. Appl. Phys.* **2004**, *95*, 3633–3639. [[CrossRef](#)]
8. Liu, J.F.; Chen, X.X.; Xu, G.S.; Yang, D.F.; Tian, Y.F.; Zhu, X. Novel high temperature ferroelectric single crystals $0.38\text{Bi}(\text{Mg}_{1/2}\text{Ti}_{1/2})\text{O}_3-0.62\text{PbTiO}_3$ with good and temperature-stable piezoelectric properties. *CystEngComm* **2015**, *10*, 5605–5608. [[CrossRef](#)]
9. Ogihara, H.; Randall, C.A.; Trolier-McKinstry, S. Weakly coupled relaxor behavior of $\text{BaTiO}_3-\text{BiScO}_3$ ceramics. *J. Am. Ceram. Soc.* **2009**, *92*, 110–118. [[CrossRef](#)]
10. Yu, H.C.; Ye, Z.G. Dielectric properties and relaxor behavior of a new $(1-x)\text{BaTiO}_3-x\text{BiAlO}_3$ solid solution. *J. Appl. Phys.* **2008**, *103*. [[CrossRef](#)]
11. Huang, C.C.; Cann, D.P. Phase transitions and dielectric properties in $\text{Bi}(\text{Zn}_{1/2}\text{Ti}_{1/2})\text{O}_3-\text{BaTiO}_3$ perovskite solid solutions. *J. Appl. Phys.* **2008**, *104*. [[CrossRef](#)]
12. Kumar, M.M.; Srinivas, A.; Suryanarayana, S.V. Structure property relations in $\text{BiFeO}_3/\text{BaTiO}_3$ solid solutions. *J. Appl. Phys.* **2000**, *87*, 855–862. [[CrossRef](#)]
13. Singh, A.; Pandey, V.; Kotnala, R.K.; Pandey, D. Direct evidence for multiferroic magnetoelectric coupling in $0.9\text{BiFeO}_3-0.1\text{BaTiO}_3$. *Phys. Rev. Lett.* **2008**, *101*. [[CrossRef](#)] [[PubMed](#)]
14. Gheorghiu, F.P.; Ianculescu, A.; Postolache, P.; Lupu, N.; Dobromir, M.; Luca, D.; Mitoseriu, L. Preparation and properties of $(1-x)\text{BiFeO}_3-x\text{BaTiO}_3$ multiferroic ceramics. *J. Alloys Compd.* **2010**, *506*, 862–867. [[CrossRef](#)]
15. Ozaki, T.; Kitagawa, S.; Nishihara, S.; Hosokoshi, Y.; Suzuki, M.; Noguchi, Y.; Miyayama, M.; Mori, S. Ferroelectric properties and nano-scaled domain structures in $(1-x)\text{BiFeO}_3-x\text{BaTiO}_3$ ($0.33 < x < 0.50$). *Ferroelectrics* **2009**, *385*, 6155–6161.
16. Wei, Y.X.; Wang, X.T.; Jia, J.J.; Wang, X.L. Multiferroic and piezoelectric properties of $0.65\text{BiFeO}_3-0.35\text{BaTiO}_3$ ceramic with pseudo-cubic symmetry. *Ceram. Int.* **2012**, *38*, 3499–3502. [[CrossRef](#)]
17. Futakuchi, T.; KaKuda, T.; Sakai, Y. Multiferroic properties of $\text{BiFeO}_3-\text{BaTiO}_3$ based ceramics. *J. Ceram. Soc. Jpn.* **2014**, *122*, 464–468. [[CrossRef](#)]
18. Leontsev, S.O.; Eitel, R.E. Dielectric and piezoelectric properties in Mn-modified $(1-x)\text{BiFeO}_3-x\text{BaTiO}_3$ ceramics. *J. Am. Ceram. Soc.* **2009**, *92*, 2957–2961. [[CrossRef](#)]
19. Yang, H.B.; Zhou, C.R.; Liu, X.Y.; Zhou, Q.; Chen, G.H.; Wang, H.; Li, W.Z. Structural, microstructural and electrical properties of $\text{BiFeO}_3-\text{BaTiO}_3$ ceramics with high thermal stability. *Mater. Res. Bull.* **2012**, *47*, 4233–4239. [[CrossRef](#)]
20. Wei, Y.X.; Wang, X.T.; Zhu, J.T.; Wang, X.L.; Jia, J.J. Dielectric, ferroelectric and piezoelectric properties of $\text{BiFeO}_3-\text{BaTiO}_3$ ceramics. *J. Am. Ceram. Soc.* **2013**, *96*, 3163–3168.
21. Singh, A.; Moriyoshi, C.; Kuroiwa, Y.; Pandey, D. Evidence for diffuse ferroelectric phase transition and cooperative tricritical freezing of random-site dipoles due to off-centered Bi^{3+} ions in the average cubic lattice of $(\text{Ba}_{1-x}\text{Bi}_x)(\text{Fe}_{1-x}\text{Ti}_x)\text{O}_3$. *Phys. Rev. B* **2012**, *85*. [[CrossRef](#)]
22. Kumar, M.M.; Suresh, M.B.; Suryanarayana, S.V.; Kumar, G.S.; Bhimasankaram, T. Dielectric relaxation in $\text{Ba}_{0.96}\text{Bi}_{0.04}\text{Ti}_{0.96}\text{Fe}_{0.04}\text{O}_3$. *J. Appl. Phys.* **1998**, *84*, 6811–6814. [[CrossRef](#)]
23. Wang, L.; Wang, X.L.; Shi, J. Measurement and estimation of ferroelectric hysteresis loops. *Ferroelectrics* **2010**, *411*, 86–92. [[CrossRef](#)]
24. Rojac, T.; Kosec, M.; Budic, B.; Setter, N.; Damjanovic, D. Strong ferroelectric domain-wall pinning in BiFeO_3 ceramics. *J. Appl. Phys.* **2010**, *108*, 074107. [[CrossRef](#)]
25. Sun, C.; Chen, X.M.; Wang, J.L.; Yuan, G.L.; Yin, J.; Liu, Z.G. Structure and piezoelectric properties of BiFeO_3 and $\text{Bi}_{0.92}\text{Dy}_{0.08}\text{FeO}_3$ multiferroics at high temperature. *Solid State Commun.* **2012**, *152*, 1194–1198. [[CrossRef](#)]
26. Yuan, G.L.; Or, S.W. Multiferroicity in polarized single-phase $\text{Bi}_{0.875}\text{Sm}_{0.125}\text{FeO}_3$ ceramics. *J. Appl. Phys.* **2006**, *100*. [[CrossRef](#)]
27. Jiang, Q.H.; Liu, F.T.; Nan, C.W.; Lin, Y.H.; Reece, M.J.; Yan, H.X.; Ning, H.P.; Shen, Z.J. High-temperature ferroelectric phase transition observed in multiferroic $\text{Bi}_{0.91}\text{La}_{0.05}\text{Tb}_{0.04}\text{FeO}_3$. *Appl. Phys. Lett.* **2009**, *95*. [[CrossRef](#)]
28. Yuan, G.L.; Baba-Kishi, K.Z.; Liu, J.M.; Or, S.W.; Wang, Y.P.; Liu, Z.G. Multiferroic properties of single-phase $\text{Bi}_{0.85}\text{La}_{0.15}\text{FeO}_3$ lead-free ceramics. *J. Am. Ceram. Soc.* **2006**, *89*, 3136–3139. [[CrossRef](#)]
29. Yuan, G.L.; Or, S.W. Enhanced piezoelectric and pyroelectric effects in single-phase multiferroic $\text{Bi}_{1-x}\text{Nd}_x\text{FeO}_3$ ($x = 0-0.15$) ceramics. *Appl. Phys. Lett.* **2006**, *88*, 1–3. [[CrossRef](#)]

30. Amorín, H.; Correas, C.; Ramos, P.; Hungría, T.; Castro, A.; Algueró, M. Very high remnant polarization and phase-change electromechanical response of $\text{BiFeO}_3\text{-PbTiO}_3$ at the multiferroic morphotropic phase boundary. *Appl. Phys. Lett.* **2012**, *101*. [[CrossRef](#)]
31. Bennett, J.; Bell, A.J.; Stevenson, T.J.; Smith, R.I.; Sterianou, I.; Reaney, I.M.; Comyn, T.P. Multiferroic properties of $\text{BiFeO}_3\text{-}(\text{K}_{0.5}\text{Bi}_{0.5})\text{TiO}_3$ ceramics. *Mater. Lett.* **2013**, *94*, 172–175. [[CrossRef](#)]
32. Cheng, J.R.; Eitel, R.E.; Cross, L.E. Lanthanum-modified $(1-x)(\text{Bi}_{0.8}\text{La}_{0.2})(\text{Ga}_{0.05}\text{Fe}_{0.95})\text{O}_3\text{-}x\text{PbTiO}_3$ crystalline solutions: Novel morphotropic phase-boundary lead-reduced piezoelectrics. *J. Am. Ceram. Soc.* **2003**, *86*, 2111–2115. [[CrossRef](#)]
33. Hu, W.; Tan, X.L.; Rajan, K. Piezoelectric ceramics with compositions at the morphotropic phase boundary in the $\text{BiFeO}_3\text{-PbZrO}_3\text{-PbTiO}_3$ ternary system. *J. Am. Ceram. Soc.* **2011**, *94*, 4358–4363. [[CrossRef](#)]
34. Fan, L.L.; Chen, J.; Li, S.; Kang, H.J.; Liu, L.J.; Fang, L.; Xing, X.R. Enhanced piezoelectric and ferroelectric properties in the BaZrO_3 substituted $\text{BiFeO}_3\text{-PbTiO}_3$. *Appl. Phys. Lett.* **2013**, *102*. [[CrossRef](#)]
35. Singh, A.; Senyshyn, A.; Fuess, H.; Pandey, D. Ferroelectric and antiferrodistortive phase transition in the multiferroic $(\text{Bi}_{0.8}\text{Ba}_{0.2})(\text{Fe}_{0.8}\text{Ti}_{0.2})\text{O}_3$: A high temperature neutron powder diffraction study. *J. Appl. Phys.* **2011**, *110*. [[CrossRef](#)]
36. Shrout, T.R.; Zhang, S.J. Lead-free piezoelectric ceramics: Alternatives for PZT? *J. Electroceram.* **2007**, *19*, 111–124. [[CrossRef](#)]
37. Craciun, F.; Galassi, C.; Birjega, R. Electric-field-induced and spontaneous relaxor-ferroelectric phase transitions in $(\text{Na}_{1/2}\text{Bi}_{1/2})_{1-x}\text{BaTiO}_3$. *J. Appl. Phys.* **2012**, *112*, 124106. [[CrossRef](#)]
38. Lalitha, K.V.; Kalyani, A.K.; Ranjan, R. Analogous stress and electric field driven structural transformation and decrease in polarization coherence on poling around the morphotropic phase boundary in $\text{BiScO}_3\text{-PbTiO}_3$. *Phys. Rev. B* **2014**, *90*, 224107. [[CrossRef](#)]
39. Damjanovic, D. A morphotropic phase boundary system based on polarization rotation and polarization extension. *Appl. Phys. Lett.* **2010**, *97*, 062906. [[CrossRef](#)]
40. Wu, J.G.; Xiao, D.Q.; Zhu, J.G. Potassium-sodium niobate lead-free piezoelectric materials: Past, present, and future of phase boundaries. *Chem. Rev.* **2015**, *115*, 2559–2595. [[CrossRef](#)] [[PubMed](#)]
41. Noblanc, O.; Gaucher, P.; Calvarin, G. Structural and dielectric studies of $\text{Pb}(\text{Mg}_{1/3}\text{Nb}_{2/3})\text{O}_3\text{-PbTiO}_3$ ferroelectric solid solutions around the morphotropic boundary. *J. Appl. Phys.* **1996**, *79*, 4291–4297. [[CrossRef](#)]
42. Muhtar, A.; Somayazulu, M.; Cohen, R.E.; Ganesh, P.; Dera, P.; Mao, H.-K.; Hemley, R.J.; Ren, Y.; Liermann, P.; Wu, Z.G. Origin of morphotropic phase boundaries in ferroelectrics. *Nature* **2008**, *451*, 545–549.
43. Cohen, R.E. Origin of ferroelectricity in perovskite oxides. *Nature* **1992**, *358*, 136–138. [[CrossRef](#)]
44. Selbach, S.M.; Tybell, T.; Einarsrud, M.A.; Grande, T. The ferroic phase transitions of BiFeO_3 . *Adv. Mater.* **2008**, *20*, 3692–3696. [[CrossRef](#)]
45. Shi, T.; Xie, L.; Gu, L.; Zhu, J. Why Sn doping significantly enhances the dielectric properties of $\text{Ba}(\text{Ti}_{1-x}\text{Sn}_x)\text{O}_3$. *Sci. Rep.* **2015**, *5*, 8606. [[CrossRef](#)] [[PubMed](#)]
46. Zhu, W.M.; Guo, H.Y.; Ye, Z.G. Structural and magnetic characterization of multiferroic $(\text{BiFeO}_3)_{1-x}(\text{PbTiO}_3)_x$ solid solutions. *Phys. Rev. B* **2008**, *78*, 014401. [[CrossRef](#)]
47. Suchomel, M.R.; Davies, P.K. Enhanced tetragonality in $(x)\text{PbTiO}_3\text{-}(1-x)\text{Bi}(\text{Zn}_{1/2}\text{Ti}_{1/2})\text{O}_3$ and related solid solution systems. *Appl. Phys. Lett.* **2005**, *86*, 262905. [[CrossRef](#)]



© 2015 by the authors; licensee MDPI, Basel, Switzerland. This article is an open access article distributed under the terms and conditions of the Creative Commons by Attribution (CC-BY) license (<http://creativecommons.org/licenses/by/4.0/>).